

1 **Total Experimental Uncertainty in Hydrodynamic Testing of a Semisubmersible Wind Turbine,**  
2 **Considering Numerical Propagation of Systematic Uncertainty**

3 Amy Robertson\*<sup>a</sup>, Erin E. Bachynski<sup>b</sup>, Sebastien Gueydon<sup>c</sup>, Fabian Wendt<sup>a</sup>, Paul Schünemann<sup>d</sup>  
4 \*Corresponding Author, email: Amy.Robertson@nrel.gov  
5

6 <sup>a</sup>National Renewable Energy Laboratory, 15013 Denver West Parkway, Golden, CO 80401

7 <sup>b</sup>Norwegian University of Science and Technology (NTNU) Department of Marine Technology, Marine  
8 Technology Center, 7491 Trondheim, Norway

9 <sup>c</sup>MARIN, 2, Haagsteeg, P.O. Box 28, 6700AA Wageningen, The Netherlands

10 <sup>d</sup> Universität Rostock, Lehrstuhl für Windenergietechnik, Fakultät für Maschinenbau und Schiffstechnik,  
11 Albert-Einstein-Straße 2, 18059 Rostock, Germany  
12

13 **Abstract**

14 Quantifying the uncertainty in experimental results is a critical step in properly validating numerical  
15 simulation tools for designing floating wind turbines; without a good understanding of the experimental  
16 uncertainties, it is impossible to determine if numerical simulation tools can capture the physics with  
17 acceptable accuracy. Recent validation studies suggest that the wave-induced, low-frequency surge and  
18 pitch motions of semisubmersible-type floating wind turbines are consistently underpredicted by  
19 numerical simulations, but it has not been possible to state whether or not this underprediction is within  
20 the level of experimental error. In the present work, previously assessed systematic uncertainty  
21 components in hydrodynamic tests of the OC5-DeepCwind semisubmersible are propagated to response  
22 metrics of interest using numerical simulation tools, and combined with the random uncertainty to obtain  
23 the total experimental uncertainty. The uncertainty in the low-frequency response metrics is found to be  
24 most sensitive to the system properties (e.g., mooring stiffness and center of gravity), but also the wave  
25 elevation. The results of the present study suggest that the underprediction of the low-frequency  
26 response behavior observed in previous validation studies is larger than the experimental uncertainty.

27 **Keywords:** Floating Offshore Wind, Uncertainty Analysis, OC5, Validation, Nonlinear Wave Mechanics

## 28 1 Introduction

29 Floating wind turbines (FWTs) represent a growing area of both academic and industrial interest, and a  
30 wide range of numerical tools have been developed to predict their responses in wind and waves.  
31 Recently, participants in the international Offshore Code Comparison Collaboration, Continued, with  
32 Correlation (OC5) project attempted to validate models of a floating semisubmersible tested in the  
33 offshore basin at MARIN (in May 2013) by the DeepCwind consortium (Goupee et al. 2014). Although  
34 state-of-the-art tools captured some of the dynamics and loads of the complex floating wind turbine,  
35 there were persistent differences between the simulated results and measurements, the reasons for  
36 which could not be ascertained.

37 The discrepancies are exemplified by an under-prediction of the ultimate and fatigue loads across multiple  
38 load cases, which were shown to be dominated by the under-prediction of the loads at the pitch and  
39 tower natural frequencies (Robertson et al. 2017). Similar discrepancies in the low-frequency response of  
40 other model-scale semisubmersible platforms for offshore wind have also been observed (Cermelli and  
41 Roddier 2005, Philippe et al. 2013, Berthelsen et al. 2016). In order to assess whether or not the observed  
42 differences between numerical and experimental results are meaningful, an assessment of the level of  
43 experimental uncertainty in the response behavior needs to be determined.

44 To that end, additional testing of the semisubmersible structure from the OC5 study (in a simplified  
45 configuration) was carried out at MARIN through the MaRINET2 grant. These simplified tests were aimed  
46 toward better understanding the hydrodynamic loading and assessing uncertainty in the test campaign.  
47 The generic open-access design (OC5-DeepCwind floating semisubmersible) was tested at 1/50 scale with  
48 the same floating substructure as was examined in OC5, but with a rigid tower, a mass representing the  
49 rotor-nacelle assembly, and with a simplified soft-spring mooring system representing the linear stiffness  
50 of the original catenary configuration. The wind turbine and flexible tower were replaced by rigid  
51 components to limit uncertainty sources and better focus on the hydrodynamic loading on the structure.  
52 Due to the limited testing time in the basin, a single configuration was considered, and a limited number  
53 of wave conditions were tested (Gueydon 2017). Extensive repetition tests were included in the test  
54 matrix to assess the random uncertainty in the experiment.

55 Response metrics, low-dimensional representations of the important features of the time series of results,  
56 are used to represent the results and the associated uncertainty. The experimental uncertainty originates  
57 from uncertainties in the excitation of the system and the properties of the test specimen, and the

58 accuracy and precision of the measurement equipment. Several standards provide guidance on  
59 uncertainty assessment, such as the International Standards Organization (ISO, 1993), American Society  
60 of Mechanical Engineers (ASME, 2013), and The International Towing Tank Conference (ITTC, 2008). Here,  
61 we apply the ASME terminology, categorizing the sources of uncertainty as either random or systematic.  
62 Systematic uncertainties may result in an unknown bias in the test, while random uncertainties result in  
63 randomly varying uncertainties which can be measured through repetition tests.

64 The contributions to the experimental uncertainty in the new set of tests were identified and documented  
65 in previous work (Robertson et al. 2018). Among the main findings, it was shown that the uncertainty in  
66 the wave elevation was small, and was dominated by the random uncertainty. It should be noted,  
67 however, that the uncertainties in the wave loads (not measured) may be larger than the uncertainties in  
68 the wave elevation. The physical properties of the model itself were found to have more significant  
69 systematic uncertainties, and the measurement cable contributed significantly to the uncertainty in the  
70 mass and in the center of mass. The measurement of motion responses was precise, while the tension  
71 measurements had relatively high random uncertainty.

72 The present work seeks to identify the total uncertainty of the response metrics of interest. This is  
73 accomplished by first propagating the systematic uncertainties to the response metrics through numerical  
74 simulations, and then combining with the calculated random uncertainty. Three state-of-the-art  
75 simulation tools – applied by four different users, and considering several modeling approaches – were  
76 used to assess the consequences of changes in the input parameters (corresponding to the systematic  
77 uncertainty levels) on responses such as the low-frequency surge and pitch motions and wave-frequency  
78 surge and pitch motions. In the remainder of the paper, the model tests and response metrics of interest  
79 are briefly described (Sections 2 and 3). Next, the uncertainty sources identified by Robertson et al. (2018)  
80 are summarized, and the most important of these are identified (Section 4). The methodology for  
81 propagating systematic uncertainties is explained, and the total uncertainty is examined (Sections 5 and  
82 6).

## 83 2 Test Description

84 The floating semisubmersible model consisted of the existing MARIN model 9697, whose geometry  
85 corresponds to the DeepCWind semisubmersible floater (Goupee et al. 2012) at 1/50 scale, and a rigid  
86 aluminum tower designed to mimic the mass and inertia of the NREL 5 MW wind turbine tower and rotor-  
87 nacelle-assembly (Jonkman et al. 2009, Jonkman 2010). A brief overview of the model setup (Figure 1) is  
88 given here; additional details may be found in Robertson et al. 2018. The test setup and all results are  
89 presented at full scale, following Froude scaling. The difference in density between sea water ( $1025 \text{ kg/m}^3$ )  
90 and fresh water in the basin ( $998.6 \text{ kg/m}^3$ ) is accounted for in the scaling of masses, inertias, forces,  
91 moments, and derived quantities.

92 A simplified mooring system was designed and constructed for the new tests. Three mooring lines,  
93 consisting of a soft spring and rigid wire, were attached to the model. A pulley system was used such that  
94 the spring could be vertical and dry, while the anchor positions were low enough that the surge-pitch  
95 coupling from the mooring system was similar to the original catenary system.

96

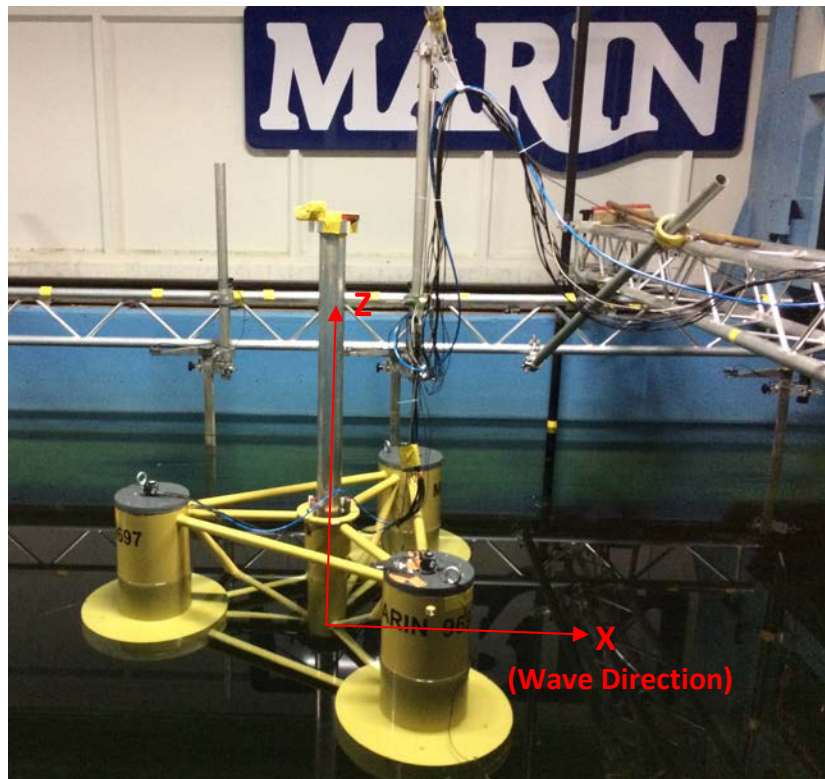


Figure 1: Floating test set-up. Waves propagate from left to right in this figure, and positive surge motion is defined in the same direction as the wave propagation (Image by: Amy Robertson).

97 2.1 Model Properties

98 The main characteristics of the floater geometry are shown in Table 1, while the hydrodynamic properties  
 99 and mass properties are given in Table 2 and Table 3, respectively. The mooring system, which included  
 100 thin wires attached to springs, is described in Table 4.

101 *Table 1: Key geometric parameters*

<b>GEOMETRIC PROPERTIES</b>	
Center column diameter [m]	6.5
Side column diameter [m]	12.0
Base column diameter [m]	24.0
Draft [m]	20.0
Base column height [m]	6.0
Side column freeboard [m]	10.0
Tower top height over keel [m]	77.3

102

103 *Table 2: Hydrodynamic properties*

<b>HYDRODYNAMIC PROPERTIES</b>	
Water depth [m]	180.0
Water density [kg/m <sup>3</sup> ]	1025.0
Displaced volume [m <sup>3</sup> ]	14040

104

105 *Table 3: Masses and inertia of entire system (tower+platform). CG: center of gravity.*

<b>MASSES/INERTIAS</b>	
Overall system mass [kg]	1.4196E+7
Overall system CG (z) [m below SWL]	7.53
Ixx abt system CG [kg-m <sup>2</sup> ]	1.2898E+10
Iyy abt system CG [kg-m <sup>2</sup> ]	1.2851E+10
Izz abt system CG [kg-m <sup>2</sup> ]	1.4189E+10

106

107 *Table 4: Mooring line properties. EA: Young's modulus multiplied by cross-sectional area.*

<b>MOORING LINES</b>	
Line angle [deg]	55.5
EA [N]	2.7106E+6
Unstretched line length [m]	55.432
Preload [kN]	1122.5

Mooring stiffness [kN/m]	48.9
--------------------------	------

108

109 When modelling the system numerically, we strived to use the properties of the system as measured,  
 110 where possible. For a floating system, the first step is to ensure that the system is in equilibrium for the  
 111 prescribed values of the draft, mass, mooring tensions, and displaced water volume. For this test, we  
 112 directly measured the draft, mass, and tensions. The displaced water volume can be calculated from the  
 113 geometry, but since it is not directly measured, we considered this property as the most unknown. We  
 114 did not tune the other properties mentioned, but prescribed the displaced water volume such that the  
 115 system was in equilibrium (Table 5).

116

*Table 5: Balance of Vertical Forces*

<b>BALANCE OF VERTICAL FORCES</b>	
Total vertical mooring force [N]	-1.9074E+06
Total gravity force [N]	-1.3922E+08
<b>Displacement needed for equilibrium [m<sup>3</sup>]</b>	<b>14040</b>
Buoyancy Force [N]	1.4113E+08
<b>SUM [N]</b>	<b>0.0000E+00</b>

117

## 118 2.2 Test Matrix

119 The tests in this campaign included a hammer test, free decay tests and wave excitation tests. Only the  
 120 wave excitation tests are of interest here, and are summarized in Table 6. As shown, multiple repetitions  
 121 were carried out for the model in waves, which will be used to assess the random uncertainty in the  
 122 response behavior. The repetitions were performed with the same wave realization, with the goal of  
 123 having identical wave time series.

124

*Table 6: Test matrix – wave cases.*

<b>Test Name</b>	<b>Waves</b>	<b>Number of repetitions</b>
Regular wave 1	H=7.1 m, T=12.1 s	5
Regular wave 2	H=4 m, T=9 s	2
White noise	Hs=7.1 m, T=6-26 s	2
Irregular wave	Hs=7.1 m, Tp=12.1 s	5

125

### 126 3 Response Metrics

127 The objective of the larger validation campaign related to these experiments is to better understand the  
128 ability of simulation tools to predict the response of the OC5-DeepCwind semisubmersible to  
129 hydrodynamic loading, especially the low-frequency (resonant) responses in pitch and surge. To assess  
130 the capabilities of the tools in this area, response metrics were identified to represent these important  
131 physical quantities of interest. The response metrics are scalar values that can be computed from the time  
132 series results from either simulations or experiments. A simulation tool that can reproduce the response  
133 metrics within the obtained uncertainty bounds can then be considered validated.

134 The response metrics in the present work focus on the surge, heave, and pitch responses of the  
135 semisubmersible, in particular: the mean response in surge, and the wave-frequency and low-frequency  
136 responses in all three degrees of freedom. The response metrics are chosen with the objective of  
137 representing these different response components, rather than selecting metrics that are useful for  
138 design (such as the 90<sup>th</sup> percentile maximum 3-hour motions), but do not distinguish among different  
139 frequency ranges.

140 The response metrics in the present work are:

- 141 M1. **RAO**: the response amplitude operator (RAO) in surge, heave, and pitch at 6 discrete frequency  
142 points within the wave energy range;
- 143 M2. **PSD Sum, Low Frequencies**: the integral of the power spectral density (PSD) of surge and pitch  
144 motions over the low-frequency range;
- 145 M3. **PSD Sum, Wave Frequencies**: the integral of the PSD of surge and pitch motions over the wave-  
146 frequency range and
- 147 M4. **Mean Surge Offset**.

148 For all of the metrics, only a limited time window of the analysis is considered (Table 7), in an attempt to  
149 focus on data after start-up transient behavior and also address the effect of reflected waves. The irregular  
150 wave window consists of the last three hours (after reflections are established), while the regular wave  
151 window includes 10 minutes of data once the ramp in the waves has passed but before any reflections  
152 arrive from the beach or wavemaker. Furthermore, all of the time series are resampled with a time step  
153 of 0.1 s prior to computing any metrics. Response metrics M2 and M3 are only computed for the irregular  
154 wave cases.

155

Table 7: Time windows for calculation of response metrics

Wave	Start of window	Duration of window
Regular wave 1	600 s	600 s
Regular wave 2	1000 s	600 s
White noise	1870 s	10800 s
Irregular wave	1870 s	10800 s

156

157 Metric M1, the RAO, is defined as the amplitude of the response divided by the amplitude of the incoming  
 158 wave at a given frequency. Six discrete frequencies are considered for the RAO calculations, as shown in  
 159 Table 8.

160

Table 8: Wave frequencies for RAO calculations

Frequency Pt.	Frequency	
1	0.065 Hz	
2	0.075 Hz	
3	0.0826 Hz	Frequency of regular wave 1
4	0.095 Hz	
5	0.105 Hz	
6	0.1105 Hz	Frequency of regular wave 2

161

162 The algorithm applied for computing the RAO, denoted  $H(\omega)$ , is based on the cross spectral density:

$$163 \quad H = \frac{yu^*}{uu^*}$$

164 where  $u$  and  $y$  are the Fourier transforms of the wave elevation and the motion response, respectively,  
 165 and the asterisk indicates the complex conjugate.

166 The integrals of the PSDs of the response (referred to as “PSD sums” – metrics M2 and M3) are chosen to  
 167 capture frequency-dependent responses both in and outside the wave frequency range in irregular sea  
 168 states. Compared to other possible metrics, such as RMS values, this approach keeps some frequency  
 169 information. When calculating the PSD sums, all time series (measured and simulated) are first cut and  
 170 sampled such that they have identical discretization in time (time step and duration). The same PSD

171 calculation algorithm, without smoothing, is then applied to all time series. The PSD sums are computed  
172 based on the one-sided, unsmoothed, discrete power density functions:

173 
$$S_{sum} = \sum_{i=j}^k S_{resp}(f_i) \Delta f$$

174 where  $S_{resp}$  is the discrete power spectral density of the response at frequency  $f_i$ ,  $\Delta f$  is the  
175 corresponding frequency increment,  $j$  is the index of the first frequency of interest, and  $k$  is the index of  
176 the last frequency of interest. The frequency limits for the low- (M2) and wave-frequency (M3)  
177 components of the spectrum are given in Table 9. These are based on identifying the ranges over which  
178 the wave spectra were defined, and then encompassing the lower frequencies below that range, without  
179 considering the zero-frequency mean value.

180 *Table 9: Frequency limits for summation of power spectral density function for response metrics M2 and M3*

Wave	Low-frequency window	Wave-frequency window
White noise	0.005 Hz – 0.038 Hz	0.038 Hz – 0.14 Hz
Irregular wave	0.005 Hz – 0.05 Hz	0.05 Hz – 0.14 Hz

181

## 182 4 Uncertainty Sources

### 183 4.1 Random Uncertainty

184 Robertson, et al. (2018) identified a number of sources for random uncertainty in the response metrics.  
185 However, since repeated measurements of the quantities of interest were available, the random  
186 uncertainty could be calculated directly from the measurements without the need to assess the source of  
187 the uncertainties. The random standard uncertainty,  $s_{\bar{x}}$ , is calculated as the standard deviation,  $s_x$ , of the  
188 metric ( $X$ ) across the repeated tests, divided by the square root of the number of observations ( $N$ ):

$$189 \quad s_{\bar{x}} = \frac{s_x}{\sqrt{N}}$$

### 190 4.2 Systematic Uncertainty

191 Systematic uncertainty is a representation of the possible bias in a test campaign, and cannot be  
192 calculated directly from measurements. Instead, the sources of systematic uncertainty throughout the  
193 test must be identified, their individual effect on the metrics calculated, and then those effects combined.  
194 The sources of uncertainty in this test campaign include the wave excitation, system properties and  
195 configuration, and output measurements. Expert analysis of the systematic uncertainties in the test  
196 campaign identified 24 separate parameters with significant levels of systematic uncertainty. These  
197 parameters are listed in Table 10. Robertson, et al. (2018) provide a thorough discussion on the  
198 assessment of the uncertainty levels for these parameters.

199 *Table 10: Sources of systematic uncertainty. CM: center of mass.*

	<b>Parameter</b>	<b>Baseline Value</b>	<b>Uncertainty Level</b>
1	Platform mass [kg]	1.4196E+7	8.75E+4
2	CM, x direction [m]	0	0.22
3	CM, y direction [m]	0	0.22
4	CM, vertical [m]	-7.53	0.21
5	Platform inertia, Ixx abt CM [kg-m <sup>2</sup> ]	1.2898E+10	1.2898E+8
6	Platform inertia, Iyy abt CM [kg-m <sup>2</sup> ]	1.2851E+10	1.2851E+8
7	Platform inertia, Izz abt CM [kg-m <sup>2</sup> ]	1.4189E+10	1.4189E+8
8	Draft [m]	20	0.25
9	Column angle, [deg]	0	0.5
10	Column diameter, [m]	12 or 24	0.1
11	Mooring stiffness [kN/m]	48.9	5.2
12	Mooring pretension [kN]	1122.5	62
13	Anchor position x [m]	Radially outward	0.25

14	Anchor position y [m]	Radially outward	0.25
15	Anchor position z [m]	Up/down	0.25
16	Mooring fairlead position [m]	Radially outward	0.05
17	Initial position [m]	0	0.12
18	Initial orientation [deg]	0	0.062
19	Water depth [m]	180	2
20	Water density [kg/m <sup>3</sup> ]	1025	10.25
21	Wave elevation – due to sensor drift [m]	measured	0.03
22	Wave elevation – due to probe location and tilt [m]	measured	negligible
23	Translation measurement [m]	0	0.03
24	Rotation measurement [deg]	0	0.3

200

201 From this original set of systematic uncertainty sources, the parameters were down-selected based on  
 202 their influence on the response metrics. They were thresholded by examining the total combined  
 203 estimated systematic uncertainty of the response metrics. Parameters whose effect on the change across  
 204 all metrics was less than 10% were removed. In the end, the original set of 24 parameters was down-  
 205 selected to 8, which are summarized in Table 11. Note that only parameters related to the system  
 206 properties and configuration remain in the list, and no measurement or wave excitation uncertainties are  
 207 included.

208

*Table 11: Selected parameters for uncertainty propagation*

	<b>Parameter</b>	<b>Abbreviation</b>
1	Center of mass, x direction	CMx
2	Center of mass, vertical	CMz
3	Mooring stiffness	Stiff
4	Draft	Draft
5	Column diameter	ColDia
6	Wave elevation – due to sensor drift	WaveElev
7	Platform inertia, I <sub>yy</sub> abt CM	I <sub>yy</sub>
8	Platform mass + Displaced Volume	Mass+Buoy

209

210 In this new list, when the platform mass was changed, the displaced volume was adjusted to ensure the  
 211 heave equilibrium position was not altered. The goal was to have each of these parameters be  
 212 independent of one another. If just the mass were altered, the draft would have changed, which is a  
 213 separate parameter.

214 Many of these variations act on the response of the system without directly changing the wave excitation.  
215 Variation 1 increases the cross-coupling of inertia contributions (surge/pitch, heave/pitch). Variations 2  
216 and 7 change the inertia moment in pitch and consequently the pitch natural period. Variation 3 results  
217 in a change of the surge natural period. On the other hand, variations 4, and 5 directly affect the wave  
218 excitation by changing the volume exposed to the waves, while also changing the pitch natural period. For  
219 variation 4, the pitch period is modified through the shift of the buoyancy point and the variation of  
220 displacement. Variation 5 results in a change in the metacentric height and hence in the pitch period.  
221 Variation 8 affects the surge and heave natural periods, while variation 6 only affects the wave excitation.

## 222 5 Uncertainty Propagation

223 “Uncertainty propagation” is determining the sensitivity of the output response to the input and model  
224 uncertainties. If a closed-form solution is known for this relationship, then the uncertainty can be  
225 propagated analytically. However, for complex problems such as the dynamics of a floating offshore wind  
226 system, a closed-form solution may not be available. In these situations, numerical methods can be used  
227 instead. A common approach is to use a Monte Carlo approach to sample the input uncertainty  
228 distribution, and calculate the effective output distribution. The calculation itself can be accomplished  
229 through simulation of a numerical model of the system. Reduced-order models are often used because  
230 of their computational efficiency, e.g., polynomial chaos expansion (Murcia, et al. 2017) and machine  
231 learning techniques (Clifton, et al. 2014). An even simpler method is sequential perturbation (Manteufel,  
232 2012 and Figliola and Beasley, 2011), which requires just two simulations at the bounds of the input or  
233 model uncertainty to assess the uncertainty bounds on the response metric of interest. Sequential  
234 perturbation is used here to limit the computation time and maintain the use of sufficiently accurate  
235 models.

236 The process of using a model to propagate uncertainty can be problematic because it relies on the use of  
237 the modeling tools that are to be validated to perform the uncertainty propagation. If the tools do not  
238 represent the phenomena of interest accurately, they may not provide an accurate assessment of the  
239 sensitivity of parameter variations on that phenomena. To address this issue, multiple numerical modeling  
240 tools and multiple modeling approaches were used to propagate the uncertainties in this work. The largest  
241 positive and negative contributions (out of all simulation approaches) are then used as the sensitivity  
242 coefficient for each parameter of interest. Within the limits of the numerical models, this approach is  
243 expected to give a conservative estimate of the uncertainty for validation purposes.

### 244 5.1 Approach

245 The systematic uncertainty of an output response metric,  $b_R$ , is calculated by combining each of the  
246 elemental systematic output standard uncertainties,  $b_i$ .

$$247 \quad b_R^2 = \sum_{i=1}^N b_i^2$$

248 For the systematic uncertainties related to the input waves or model properties, these uncertainty values  
249 ( $d_i$ ) must be first propagated to their effect on the response metric uncertainty:

250

$$b_i = \theta_i d_i$$

251 where  $\theta_i = \partial X / \partial p_i$  are the sensitivity coefficients of individual parameters,  $p_i$ , on the metric of interest,  
252  $X$ ; and,  $d_i$  are the elemental input/model systematic uncertainties (as summarized in Table 11). Once  
253 propagated, each of the output metric uncertainty sources may be summed. The sensitivity coefficients  
254 represent the influence that the input/model uncertainties have on the output metrics, and are typically  
255 calculated analytically; but, if that is not possible, numerical models of the system can be used to estimate  
256 them.

257 In this work, the systematic uncertainty of the response metrics due to a given uncertainty source is  
258 estimated by sequential perturbation by first simulating the model using the baseline properties and  
259 calculating the associated response metrics. Then, the system is simulated using a new value for one of  
260 the six uncertain parameters, based on the uncertainty level described in Table 11 (changes are made in  
261 both the positive and negative directions), and the response metrics are again calculated. The difference  
262 between the response metrics calculated using the baseline properties and when changing one of the  
263 uncertain parameters is the systematic uncertainty for that parameter. Systematic uncertainties will be  
264 calculated based on both a positive and negative change in the parameter, and the resulting level of  
265 propagated uncertainty may not be the same (see Section 5.2). This process is repeated for all six  
266 parameters, and then those individual uncertainty sources combined in quadrature. This method assumes  
267 that each of the systematic uncertainty sources in Table 11 are independent of each other.

## 268 5.2 Asymmetric Uncertainty

269 The propagation results in non-symmetric uncertainty bounds for the metrics; meaning that the  
270 uncertainty on the positive end is sometimes different from the level on the negative end of the metric  
271 value. This situation creates a complication in combining the different systematic uncertainty sources as  
272 the straightforward method of adding them in quadrature no longer works. Different approaches can be  
273 used to address this. The simplest approach is to add the negative uncertainty bounds in quadrature, and  
274 the positive uncertainty bounds in quadrature, separately; but, this approach has been shown to be  
275 inaccurate. Another approach is proposed by Dieck (2007) and uses the calculation of a central value for  
276 the nonsymmetric uncertainty bounds, which is then used to adjust the final uncertainty summed across  
277 multiple sources. This approach was used here. The systematic response metric uncertainty,  $b_i$ , for an  
278 individual parameter ( $i$ ) is calculated as:

279

$$b_i = \frac{(\bar{X} + b_i^+) - (\bar{X} - b_i^-)}{2}$$

280  
281  
282

where  $\bar{X}$  is the mean measured value for a given metric. The total estimated systematic standard uncertainty,  $b_R$ , is then calculated. The asymmetry of the systematic uncertainty is further addressed in the calculation of the total uncertainty (Section 6.1).

### 283 5.3 Modeling Tools / Methods

284  
285  
286  
287  
288  
289  
290

Three different simulation tools were used to propagate the systematic uncertainty in the model properties to the response metrics, and several different users contributed results. A variety of tools and users was employed since the approach used to model the behavior of the floating wind system may affect the propagation of uncertainty. Ideally, the modeling tools that are to be validated would not be the same ones used to perform the uncertainty propagation, but this is the only option for a complex system such as a floating wind turbine. The largest propagated uncertainty found across the different tools and users was used to help assuage this limitation.

291  
292  
293  
294  
295  
296  
297  
298  
299  
300

All of the simulation approaches represent the floating wind system as a rigid body with linear elastic mooring lines. For the hydrodynamic loading, second-order diffraction is considered in addition to first-order potential flow contributions (added mass, radiation damping, and excitation). The smaller braces and pontoons were ignored in the potential flow solution. Different meshes and potential flow solvers were used (WAMIT – WAMIT, 2011 and DIFFRAC – Buchner, 2001), and so the first- and second-order potential flow solutions differ among the simulation approaches. Overall, when the same modeling approach is used (but different modeling tools), there is reasonable agreement of the wave and low-frequency motions (Gueydon et al, 2014); however, differences in the modeling of the first-order and second-order wave excitations and damping lead to differences in the motion responses, especially around the resonance frequencies in surge, heave and roll/pitch (Robertson et al, 2017).

301  
302  
303  
304  
305  
306  
307

For this study, five modeling approaches were followed with three distinct simulation tools to propagate deviations in the set of parameters of Table 11. The main differences between these modeling approaches are summarized in Table 12. Two fundamentally different approaches were used to account for linear and quadratic damping effects. A subset of the numerical models used Morison-type drag to compute quadratic damping loads on the substructure members (FAST, SIMA, aNySIM), while another subset of models used a tuned linear (P) and quadratic damping (Q) matrix (FAST\_PQ, aNySIM\_PQ), also referred to as the PQ-approach in this paper. The tuning was conducted based on decay tests in surge, heave and

308 pitch. The PQ-approach was included here because it has demonstrated improved model predictions for  
 309 the low-frequency pitch motion response of the system in past projects (Gueydon, 2016). The  
 310 corresponding damping matrices are shown in Table 13.

311 *Table 12: Numerical modelling approaches*

Model ID	Global linear and quadratic drag	Morison drag on vertical columns	Morison drag on heave plates	Wave loads above still water level
FAST		x	x	Morison-type drag up to 1 <sup>st</sup> order free surface based on constant potential
FAST_PQ	x			
SIMA		x	x	Morison-type drag up to 1 <sup>st</sup> order free surface based on constant potential
aNySIM			x	Morison loads applied on heave plate only, Therefore, no wave loads act above still water level.
aNySIM_PQ	x			

312  
 313 *Table 13: Global linear and quadratic damping coefficients applied in the PQ modelling approaches.*

DOF	Linear Damping	Quadratic Damping
Surge	1.83E+5 N/(m/s)	0.0 N/(m/s) <sup>2</sup>
Heave	0.0 N/(m/s)	3.04E+6 N/(m/s) <sup>2</sup>
Pitch	6.47E+7 Nm/(rad/s)	2.26E+10 Nm/(rad/s) <sup>2</sup>

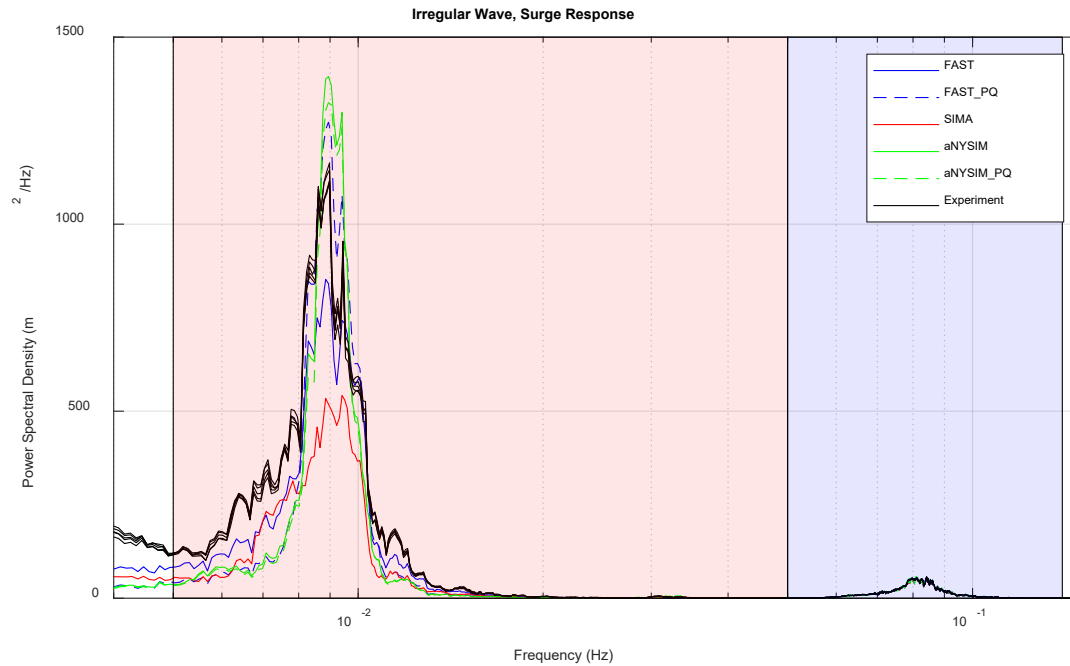
314  
 315 Furthermore, the models using Morison elements don't apply the coefficients identically: the location of  
 316 these elements and values of the coefficients are different. While all five models accounted for second-  
 317 order difference frequency diffraction, the quadratic transfer functions (QTF) are different. The quadratic  
 318 terms of the QTF used in the aNySIM and aNySIM\_PQ simulations were updated based on the motion  
 319 RAO of the floater of the present study, while all other simulations were performed with QTFs based on  
 320 the OC5-DeepCwind system (Robertson et al. 2017). Even though none of these models is perfect, it is  
 321 assumed that the choice of several tools and modeling approaches should enable an assessment of

322 realistic trends for the propagation of the uncertainty linked to the 8 most influential parameters of Table  
323 11.

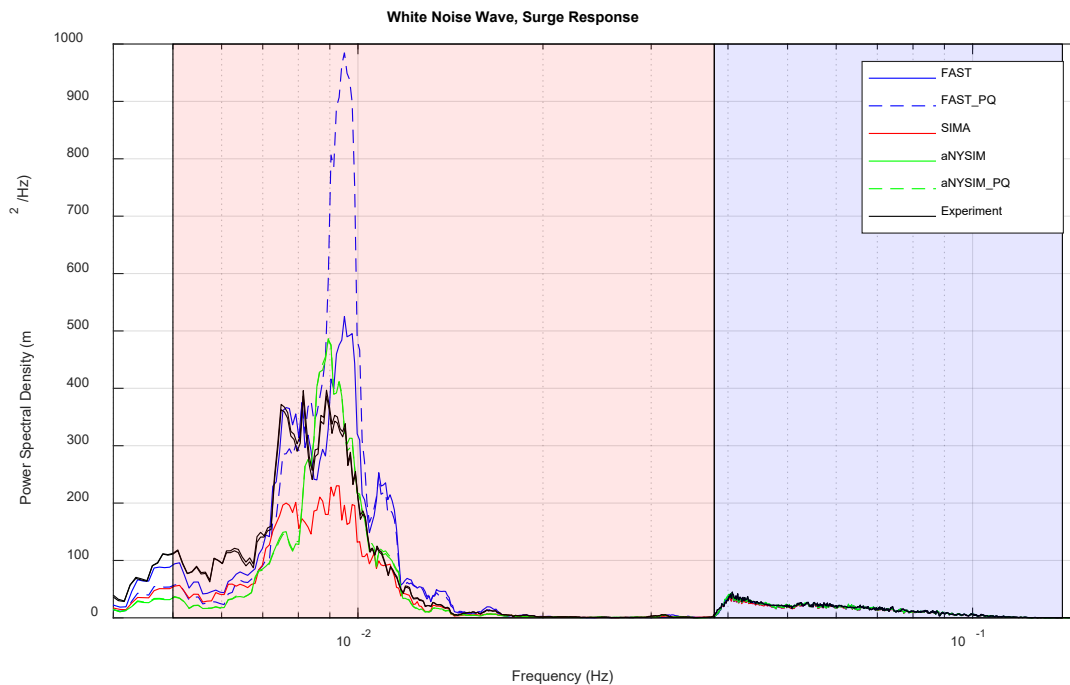
324 Figure 2- Figure 5 show a comparison of the PSDs of the surge and pitch responses for the experimental  
325 measurements and the baseline simulations. The integration limits for the low-frequency and wave-  
326 frequency PSD sums are illustrated using the colored pink and blue regions in the plots. As shown, the  
327 responses around the natural frequencies in surge ( $\sim 0.01$  Hz) and pitch ( $\sim 0.03$  Hz) are significant  
328 compared to the wave-frequency responses, and the experimental measurements show high levels of  
329 repeatability in the experiments. Figure 6 compares the PSD sum metrics (calculated from these values)  
330 between experiment and baseline simulations.

331 The wave-frequency surge and pitch responses are captured fairly well by all of the approaches, though  
332 the PQ approaches tend to underpredict the pitch response in this frequency range. Due to the resonance,  
333 small deviations of the wave loads and/or the damping can result in differences among simulations. Every  
334 modeler was free to choose his/her own approach to account for the damping and the wave excitation.  
335 As a consequence, the predictions of the responses around the resonance frequencies in surge and pitch  
336 are far less consistent between the different simulation tools than those in the wave-frequency region, as  
337 evident from the response metrics in Figure 6.

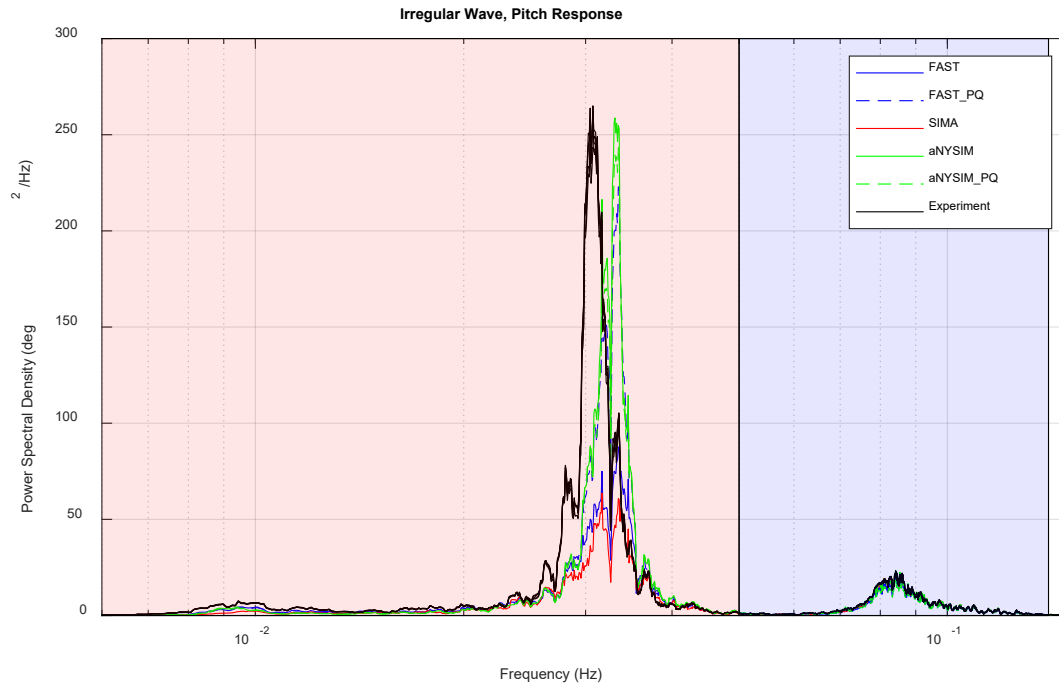
338 This discrepancy represents an important limitation in the propagation of systematic uncertainty through  
339 the use of simulation models. Can a simulation tool accurately propagate uncertainty in a metric that it  
340 does not accurately represent? As shown in Figure 6, there is varying levels of agreement for the low-  
341 frequency PSD sums between simulation and experiment, with the simulations sometimes over-predicting  
342 the metric value (e.g., FAST and FAST\_PQ for the white noise cases), but mostly under-prediction. Since  
343 there is a reasonable level of agreement for some tools, it is assumed that the physics included in the  
344 numerical simulation tools should be able to capture the relative change in platform responses due to  
345 small modifications in the input. The consistency of the propagated uncertainty between different  
346 modeling approaches will later be examined to assess the validity of this statement.



347  
 348 *Figure 2: Power spectral density (log scale abscissa) of platform response in surge for irregular wave excitation; pink shading*  
 349 *indicates low-frequency range for metric definition and blue indicates wave-frequency range. All experimental realizations are*  
 350 *shown.*

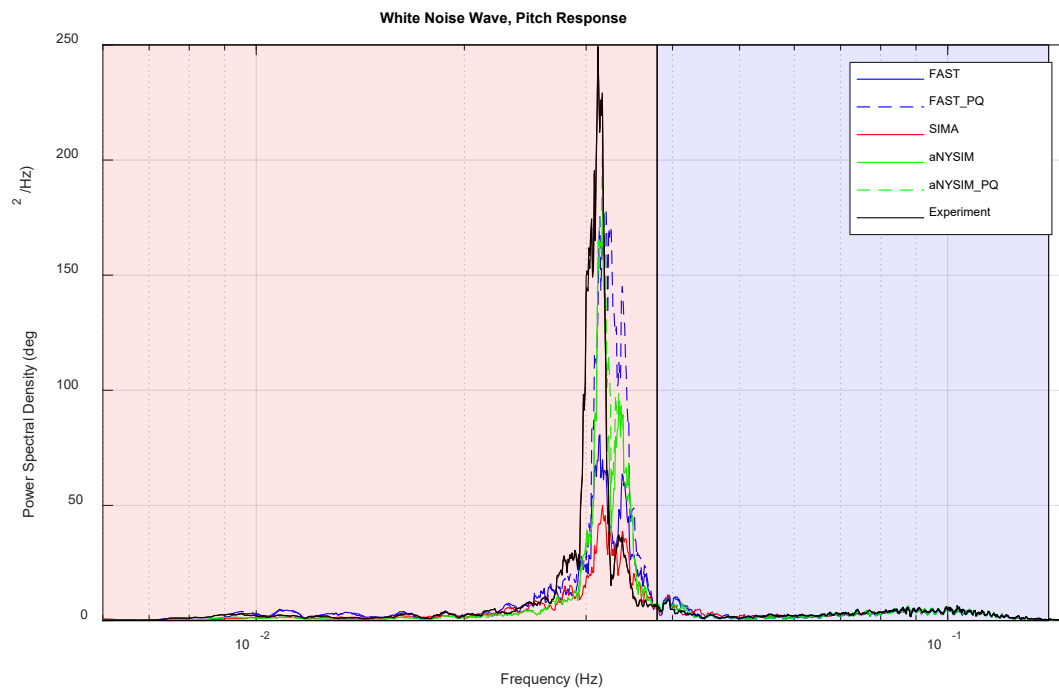


351  
 352 *Figure 3: Power spectral density (log scale abscissa) of platform response in surge for white noise wave excitation; pink shading*  
 353 *indicates low-frequency range for metric definition and blue indicates wave-frequency range. All experimental realizations are*  
 354 *shown.*



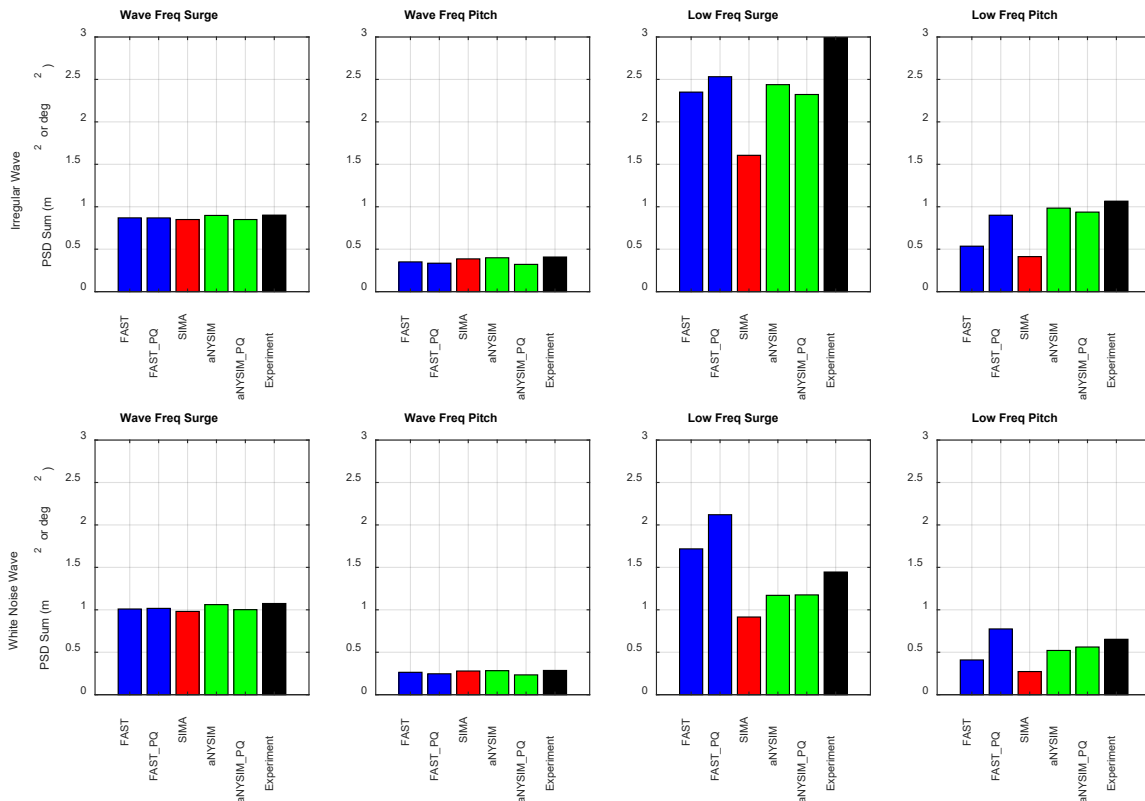
355

356 *Figure 4: Power spectral density (log scale abscissa) of platform response in pitch for irregular wave excitation; pink shading*  
 357 *indicates low-frequency range for metric definition and blue indicates wave-frequency range. All experimental realizations are*  
 358 *shown.*



359

360 *Figure 5: Power spectral density (log scale abscissa) of platform response in pitch for white noise wave excitation; pink shading*  
 361 *indicates low-frequency range for metric definition and blue indicates wave-frequency range. All experimental realizations are*  
 362 *shown.*



363  
364

Figure 6: PSD sums: comparison of baseline simulations and measurements.

### 365 5.4 Implementation of Parameter Variations in Numerical Models

366 The parameter variations considered for the assessment of the systematic uncertainty were implemented  
 367 with different approaches in the different numerical models. Differences arose because every numerical  
 368 model has inherently different ways of specifying key modelling parameters. The goal was to isolate  
 369 modifications to the model properties to only one parameter at a time; but, based on the modeling  
 370 approach employed, this was not always possible. The different realizations of the model parameter  
 371 variations for each modelling tool are outlined below.

372 **Variation 1)** CM, x direction, **Variation 2)** CM, z direction, **Variation 7)** Inertia, Iyy

373 The systematic uncertainty related to variations in the offset of the system center off mass in the x- and  
 374 z-directions is investigated with Variation-1 and Variation-2. The x-offset value was specified as +/- 0.22  
 375 m and the z-offset was specified as +/-0.21 m respectively.

376 FAST and SIMA: For the CM change, only the CM is moved, there is no change in the moment of inertia.

377 Similarly, for Variation 7, only the inertia is changed.

378 aNySIM: In MARIN's simulation tool, the inertia moments are defined at the center of mass. As a  
379 consequence, shifting the CM resulted in a change of moments of inertia. For instance,  
380 Variation 1 resulted in a change in the pitch period of about 2%. For variation 7, the inertia  
381 is changed independently of the mass by defining a new radius of inertia for the pitch  
382 rotation. The pitch period varied of 0.3% as a result of this inertia variation.

### 383 **Variation 3) Mooring stiffness**

384 For Variation 3, the systematic uncertainty related to variations in the mooring stiffness is investigated.

385 FAST and SIMA: For Variation 3, the mooring line stiffness was varied by changing EA together with  
386 the unstretched line length (+/- 2.732 m) to ensure that the mooring pre-tension did not  
387 change.

388 aNySIM: Variation 3 led to a small change of the pitch period of about 0.02%. The simulation tool  
389 accepts the stiffness and pre-tension directly as input parameters while the unstretched  
390 length is automatically adjusted.

### 391 **Variation 4) Draft, Variation 5) Column diameter**

392 The systematic uncertainty related to variations in the platform draft (+/- 0.25 m) and column diameter  
393 (+/- 0.1 m) are investigated with Variation 4 and Variation 5.

394 FAST and SIMA: To model the impact of changes in the platform draft and column diameter on the  
395 hydrodynamic loads without adjusting any additional model parameters (e.g. mass or line  
396 tension), the first-order potential flow solution was updated by adjusting the platform  
397 geometry mesh that is used in WAMIT. This leads to updated hydrodynamic databases for  
398 the radiation and diffraction loads. The hydrostatic restoring matrix is also updated to  
399 account for the changes in buoyancy force, center of buoyancy, and waterplane moment of  
400 inertia. The Morison-type drag forces on the columns were also updated to reflect the  
401 changes in geometry. Note that the 2<sup>nd</sup>-order solution was not updated.

402 aNySIM: For variations 4 and 5, the corresponding change of volume was used to scale the potential  
403 flow database based on the displacement. For the draft variation, the volume was estimated  
404 to vary by 0.7%. For the column diameter variation, the volume was estimated to vary by  
405 1.2%. Froude scaling was applied to all quantities resulting from the potential flow

406 calculation (i.e. 1<sup>st</sup> order quantities and the quadratic transfer functions). The linear  
407 hydrostatics were updated based on the new submerged geometry (displacement, center of  
408 buoyancy, waterline area second moment) while the position of the center of mass with  
409 respect to the keel was kept unchanged. When used, the diameter of the Morison elements  
410 representing the heave plates was changed with the same value as the diameter of the  
411 columns.

#### 412 **Variation 6) Wave Elevation**

413 ALL: A potential 3 cm drift in the wave elevation measurement was estimated based on  
414 measurements before and after the wavemaker started. This uncertainty was addressed by  
415 adjusting the input wave elevation by a multiplicative factor. This multiplicative factor  
416 considered the 3 cm drift as the error in a representative wave amplitude. For the irregular  
417 waves with 7.1 m Hs, this factor was thus  $1 \pm 0.00845$ .

#### 418 **Variation 8) Mass**

419 FAST and SIMA: The mass of the floater was adjusted based on the assessed uncertainty. To avoid  
420 changing the draft of the structure, another parameter needed to be adjusted to achieve the  
421 same equilibrium position. Since the displaced volume of the structure was not directly  
422 measured, it was determined to alter this value in conjunction with the mass. The displaced  
423 volume was altered by  $\pm 85.4 \text{ m}^3$  in order to maintain the same equilibrium position. The  
424 wave excitation loads were not modified due to the change in volume.

425 aNySIM: In the same way as for FAST and SIMA, the displacement was modified in conjunction with  
426 the mass to avoid changing the draft. Moreover, the radius of inertia was altered to keep the  
427 moment of inertia unchanged. This was done for roll, pitch and yaw.

## 428 6 Total Uncertainty

### 429 6.1 Combining all uncertainty sources

430 Once the total estimated systematic and random uncertainty values are calculated, they are combined to  
431 determine the total combined uncertainty,  $u_C$  for a given output metric:

$$432 \quad u_C = \sqrt{(b_R)^2 + (s_{\bar{x}})^2}$$

433 Confidence intervals are then assigned to this uncertainty to define the expanded uncertainty ( $U$ ):

$$434 \quad U = k u_C$$

435 where  $k$  is the coverage factor. When the expected distribution of the measured data is approximately  
436 normal and the effective degrees of freedom (DOF) are large, confidence intervals of 95% to 99% are  
437 typically used, which results in a coverage factor of approximately 2 to be applied to the uncertainty bound  
438 (Kim and Hermansky, 2014). A representation of a response metric,  $X$ , is then given as:

$$439 \quad X = \bar{X} \pm U$$

440 where  $X$  is the best available estimate of the measurement,  $\bar{X}$  is the mean of the response metric,  $U$  is the  
441 expanded uncertainty, and  $X-U$  and  $X+U$  define the uncertainty bounds that would include a large portion  
442 of the possible occurrences of the response metric.

443 However, when there is asymmetry in the uncertainties, the definition of the expanded uncertainty  
444 bounds must be adjusted. This is accomplished by defining a displacement,  $q$ , between the center of each  
445 nonsymmetrical systematic uncertainty interval and the average:

$$446 \quad q_i = \frac{(\bar{X} + b_i^+) + (\bar{X} - b_i^-)}{2} - \bar{X}$$

447 This displacement value is used to reinsert the asymmetry so that the total uncertainty interval is  
448 nonsymmetrical:

$$449 \quad X = \left( \bar{X} + \sum_{i=1}^N q_i \right) \pm U$$

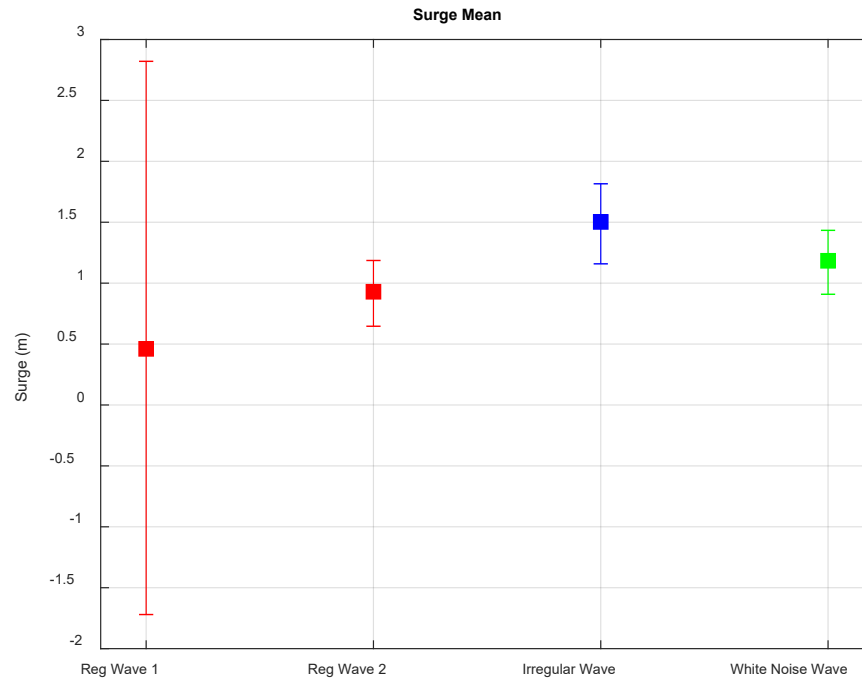
450 When there is more than one nonsymmetrical uncertainty source, the  $q$  values are summed algebraically  
451 to provide an overall asymmetry level across all nonsymmetrical sources.

452 In the present work, when accounting for the uncertainty contributions from different simulation tools,  
453 the largest positive and negative contributions (out of all simulation approaches) are kept for each  
454 parameter variation.

## 455 6.2 Total uncertainty values

456 The calculated uncertainty values for each of the four metrics are shown in Figure 7 - Figure 9. The mean  
457 metric values, shown as a square, are calculated from the response measurements averaged over all of  
458 the repeated tests. The calculated uncertainty bands are shown using error bars, and represent the  
459 expanded uncertainty ( $\pm U$ ) that includes both systematic and random uncertainty sources.

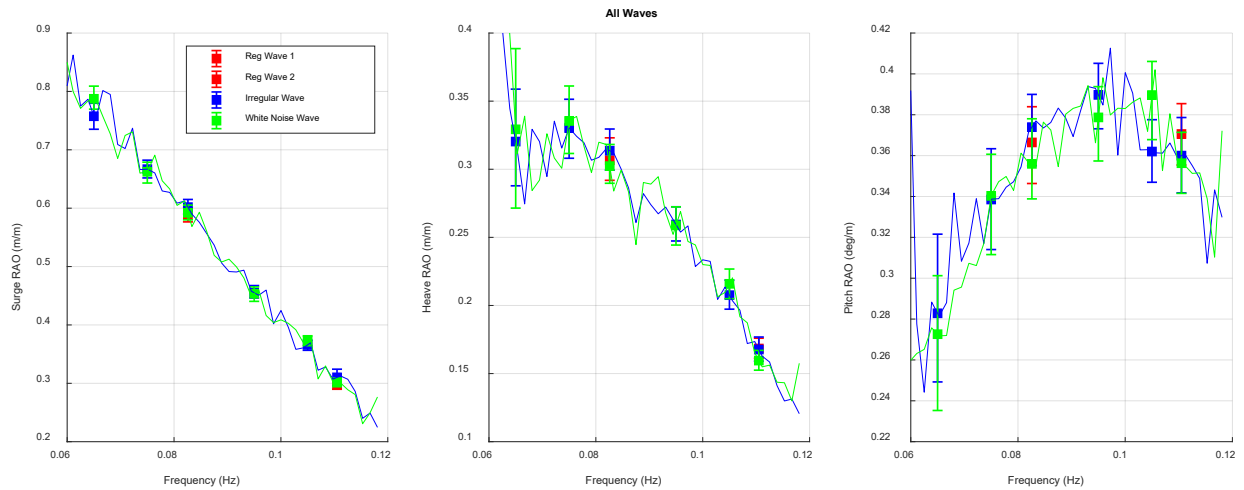
460 Figure 7 shows significant uncertainty in the mean surge metric, especially for the regular wave cases. The  
461 mean surge value was typically small, so small changes due to parameter variations can create significant  
462 levels of uncertainty in this metric. The main source of the uncertainty in mean surge position was related  
463 to the center of mass in the x-direction (CM<sub>x</sub>) for regular wave case 1, while the mooring pretension and  
464 stiffness also contributed for the other waves. The uncertainty in mean surge in regular wave case 1 is  
465 probably overstated: the large variation was only seen for one of the simulation tools, and much of the  
466 difference is likely related to static effects (which would have been zeroed out in the experimental  
467 measurements).



468

469 *Figure 7: Mean surge metric for each wave case. The square indicates the mean value across all repeat tests, and error bars*  
 470 *indicate the uncertainty bounds*

471 Figure 8 shows the experimentally obtained RAOs for the irregular and white noise waves – averaged over  
 472 the repetitions and smoothed. Plotted on top of these curves are the six frequency points computed for  
 473 each of the waves, including the expanded uncertainty. Where multiple repetitions are available, the  
 474 mean of all of the repetitions is shown. There is generally good agreement in the experimentally obtained  
 475 RAOs between different wave conditions. Although some larger discrepancies can be observed in the pitch  
 476 RAO at a given frequency, individual wave RAO values fit within the error bars for other wave RAO values.  
 477 The uncertainty level depends on the frequency. The uncertainty in the low-frequency responses is larger  
 478 than the uncertainty at higher frequencies. The trend toward higher uncertainty at low frequencies is  
 479 observed in most of the uncertainty parameters, suggesting that the main reason may be related to the  
 480 increasing importance of 1) damping since the excitation frequency approaches the natural frequency  
 481 (especially in heave and pitch) and 2) cancellation effects in the excitation (which depend strongly on the  
 482 geometry). Although the uncertainty level at a given frequency is similar for all considered waves, it is not  
 483 identically reproduced. The main conclusions from Figure 8 are that the uncertainty in the wave-frequency  
 484 responses is generally small for wave periods shorter than approximately 14 seconds, and that the pitch  
 485 responses are more uncertain than surge responses.



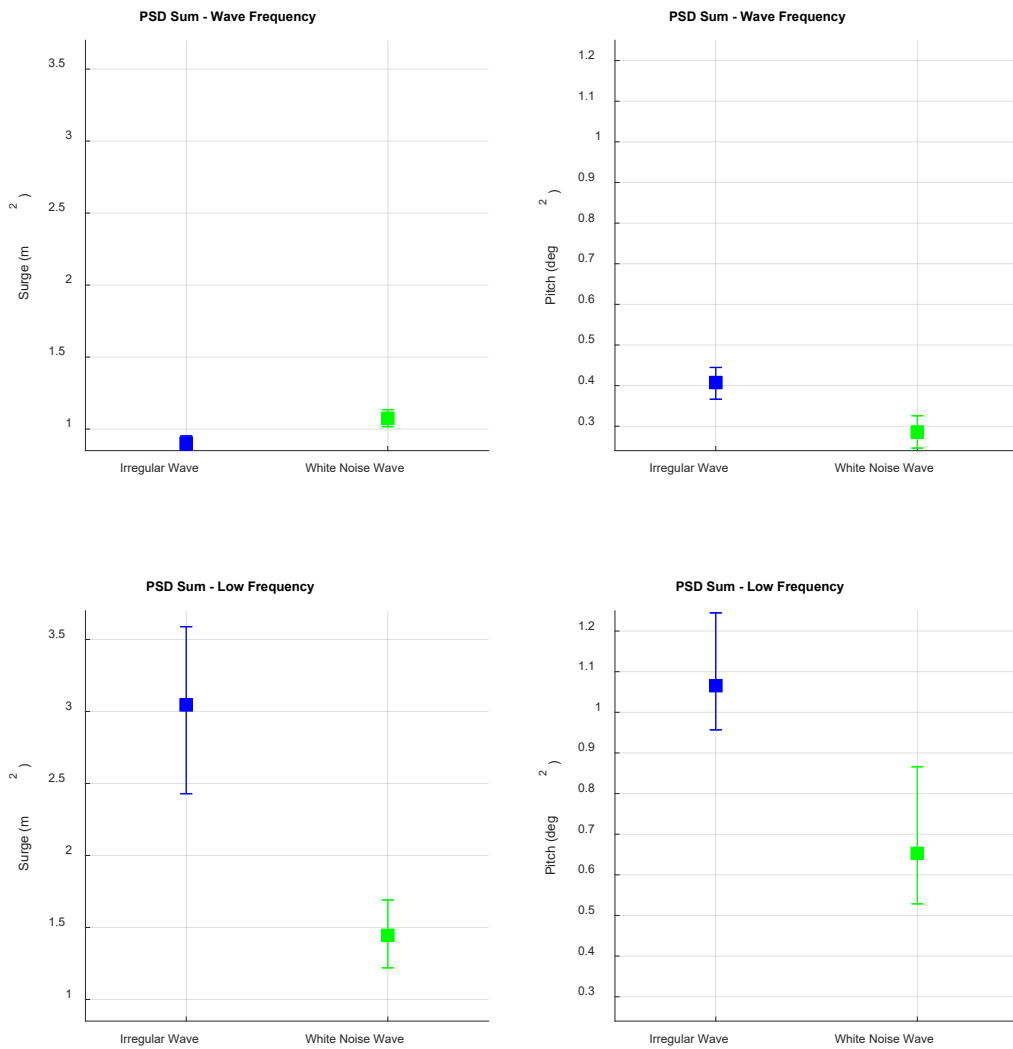
486

487 *Figure 8: Comparison of RAO values across wave cases. Mean results at the selected frequencies (for each wave) are shown by*  
 488 *squares, and error bars indicate the uncertainty bounds for those frequencies. Lines show the experimentally obtained RAOs by*  
 489 *irregular and white noise waves.*

490 The focus of this test campaign is on the low-frequency response of the wind turbine in the surge and  
 491 pitch DOFs. Figure 9 shows the PSD sum metric for both the irregular and white noise wave in these two  
 492 DOFs in both the wave and low-frequency regions. The uncertainty levels vary between the two irregular  
 493 waves (irregular and white noise); the difference is especially pronounced in the low-frequency surge  
 494 metric. The amplitude of the total uncertainty in the wave-frequency PSD sum metric is less than 20%,  
 495 while the low-frequency PSD sum metric for surge is on the order of 30-50% and the low-frequency PSD  
 496 sum metric for pitch is approximately 40% for the white noise wave case.

### 497 6.3 Contributions to uncertainty

498 To understand what is driving these uncertainties, the individual uncertainty sources ( $b_i$  and  $s_{\bar{x}}$ ) are shown  
 499 in Figure 10. This figure indicates that the high uncertainty levels in the surge direction come from  
 500 uncertainty in the mooring stiffness for the low-frequency response and from the wave elevation, column  
 501 diameter and mass/buoyancy for the wave-frequency response. In the pitch direction, uncertainty in the  
 502 center of mass offset, and also column diameter and draft, create the largest levels of uncertainty in the  
 503 response. These results highlight the fact that the low-frequency responses, which are primarily resonant  
 504 responses, are especially sensitive to parameters that affect the stiffness of the system and the inertia of  
 505 the system. Changes in stiffness or changes in inertia may shift the natural frequency slightly, and the level  
 506 of excitation at the resulting natural frequency may differ compared to the original system. Figure 10 also  
 507 confirms that the contribution of the random uncertainty to the total uncertainty is negligible compared  
 508 to the systematic uncertainty.



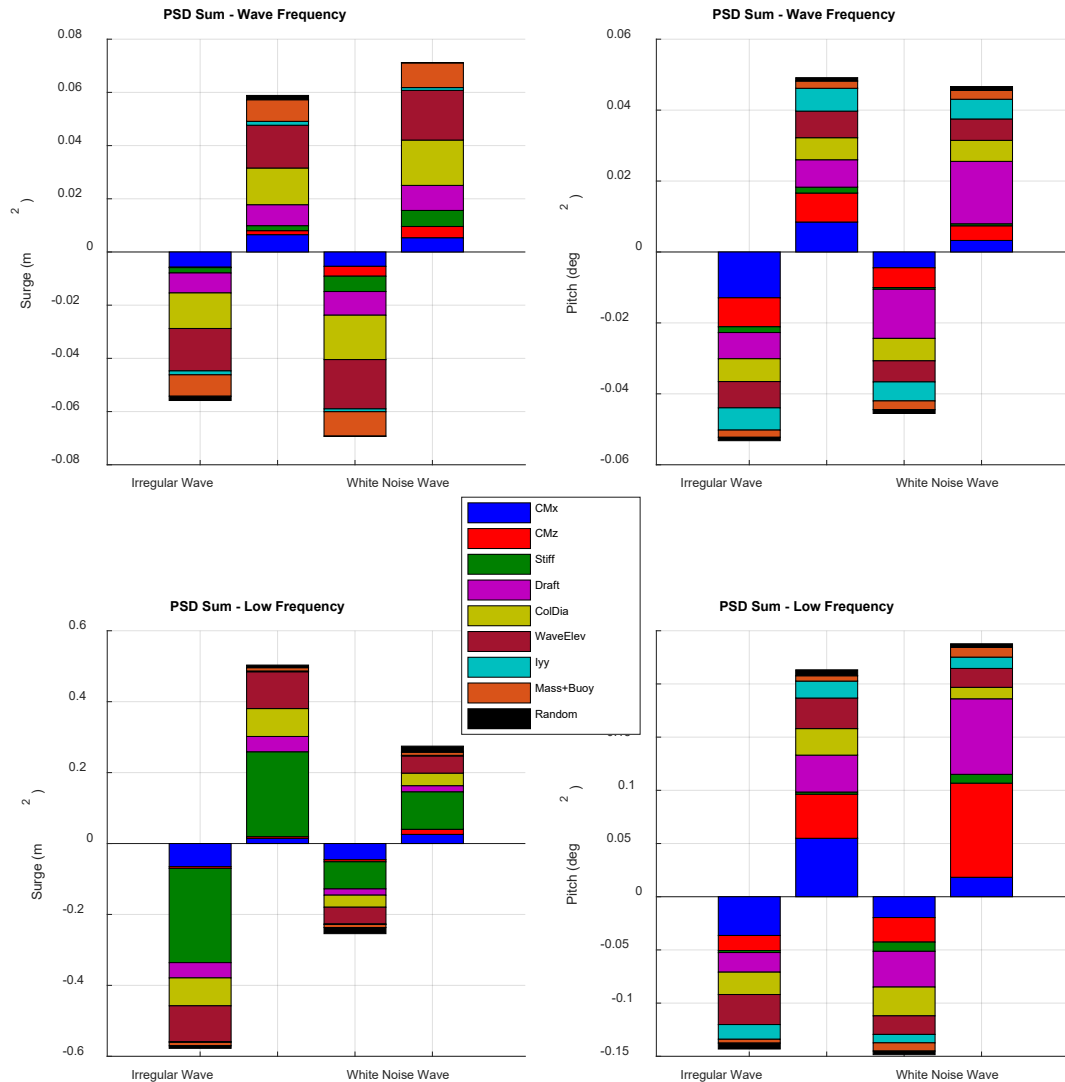
509

510 *Figure 9: PSD sum metrics for the irregular and white noise wave cases, in both pitch and surge directions; square indicates the*  
 511 *mean value across all repeat tests, and bars indicate the uncertainty bounds*

512

513

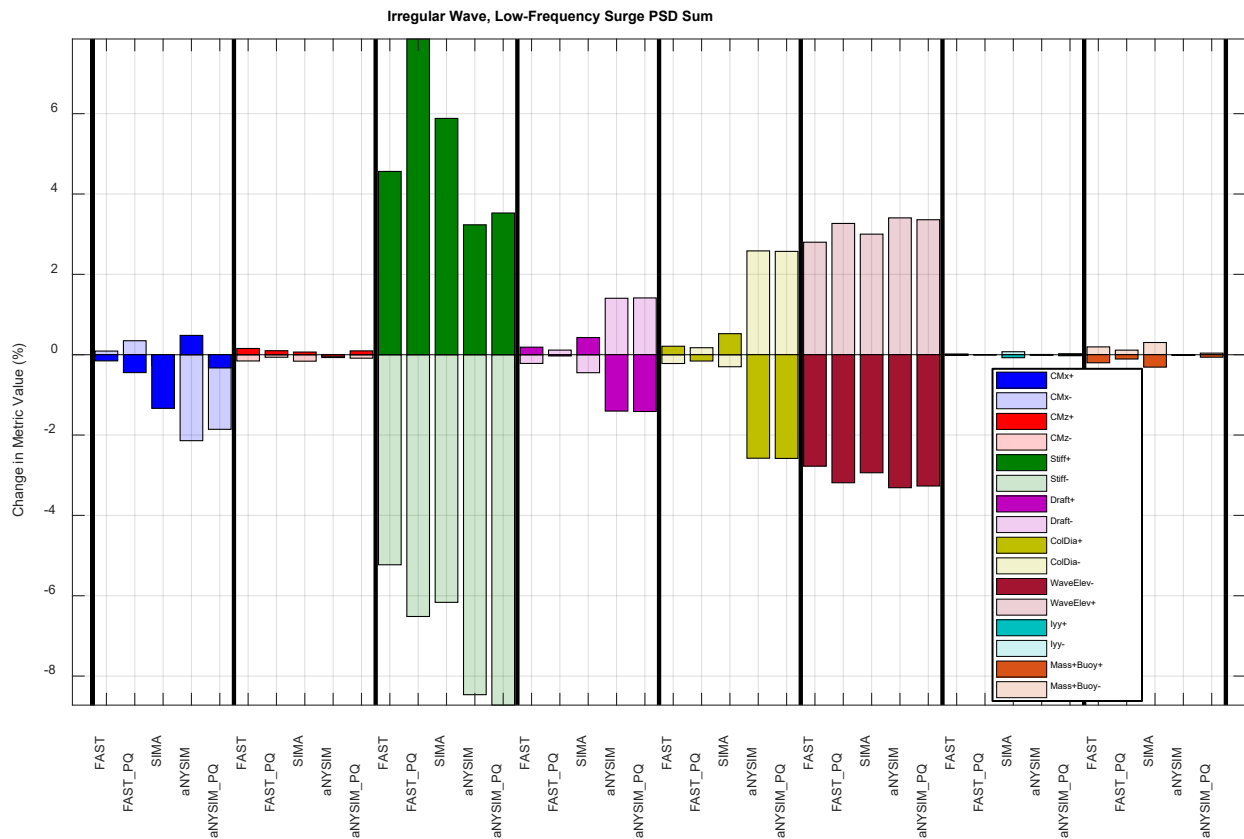
514



515  
 516 *Figure 10: Break-down of sources of uncertainty (random and individual systematic sources) for the PSD sum metric*

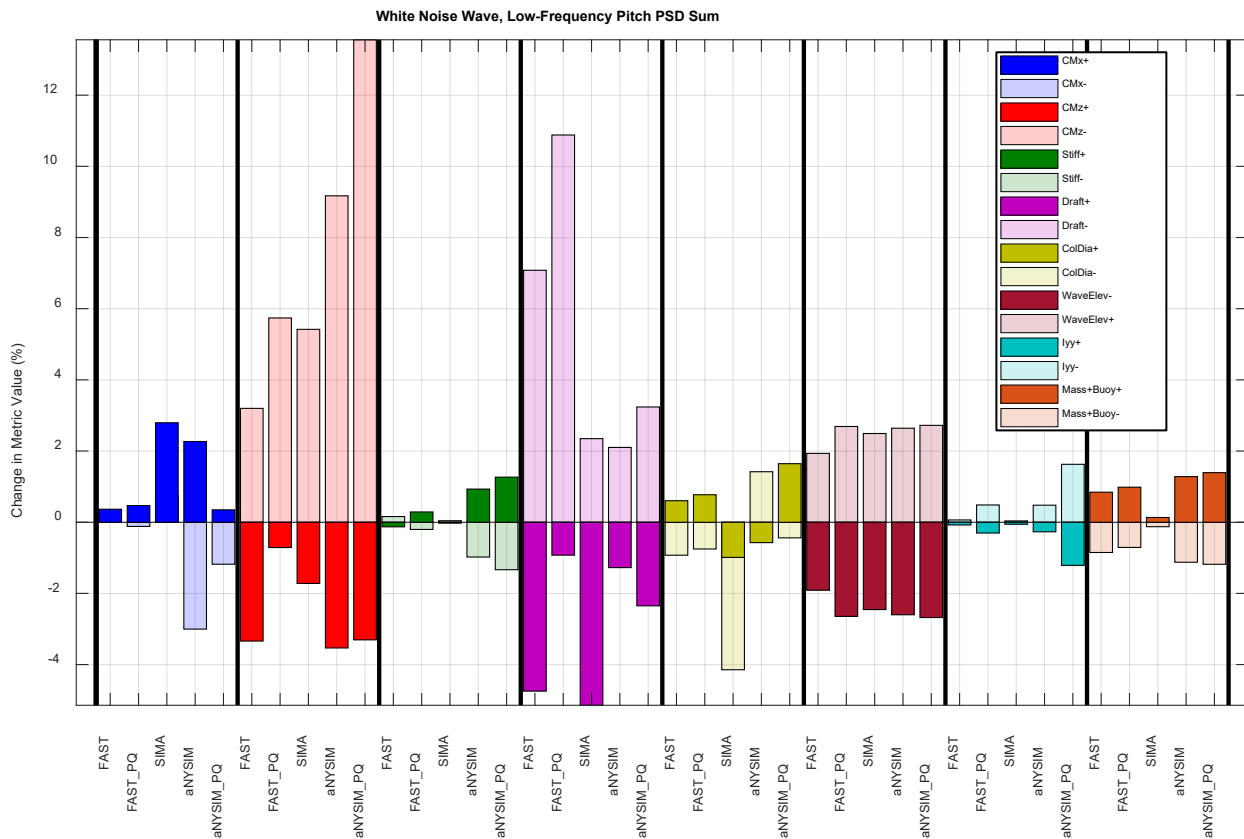
517 Figure 11 and Figure 12 examine the variability in the level of propagated uncertainty for these uncertainty  
 518 sources based on what modeling tool is used, considering two of the low-frequency response metrics with  
 519 large uncertainty: surge in the irregular wave in Figure 11 and pitch in the white noise wave in Figure 12.  
 520 The contributions from each tool for each parameter variation, both positive and negative, are included.  
 521 The different simulation tools generally agree regarding *which* parameters give the largest contributions  
 522 to uncertainty, such as the mooring stiffness and pretension for the low-frequency surge, and mostly  
 523 agree on the direction of the largest changes (i.e. positive or negative change in the metric). On the other  
 524 hand, there are significant variations in the magnitude of the changes in the metric depending on which  
 525 simulation tool is applied.

526 It is important to note that the changes in metrics from different parameter variations are additive, and  
 527 that only the largest variations (among different simulation tools) are used in the calculation of total  
 528 uncertainty. As a result, the total uncertainty in this study is more conservative than if one had only used  
 529 a single simulation tool. There is not a clear pattern suggesting that the PQ- or Morison-type approaches  
 530 give larger uncertainty for particular parameter variations, but a closer correlation can be noted based on  
 531 simulations using the same modelling tools (comparing, for example, surge results with aNySIM\_PQ and  
 532 aNySIM, or results from FAST and FAST\_PQ). Nonetheless, it is impossible to determine whether or not  
 533 the use of engineering models to predict low-frequency responses will give a conservative or non-  
 534 conservative estimate of the total uncertainty.



535

536 *Figure 11: Variability of propagated uncertainty for the irregular, low-frequency surge PSD sum metric, based on a variety of*  
 537 *modelling approaches; positive metric variations are in bold and negative are shown in a muted color*

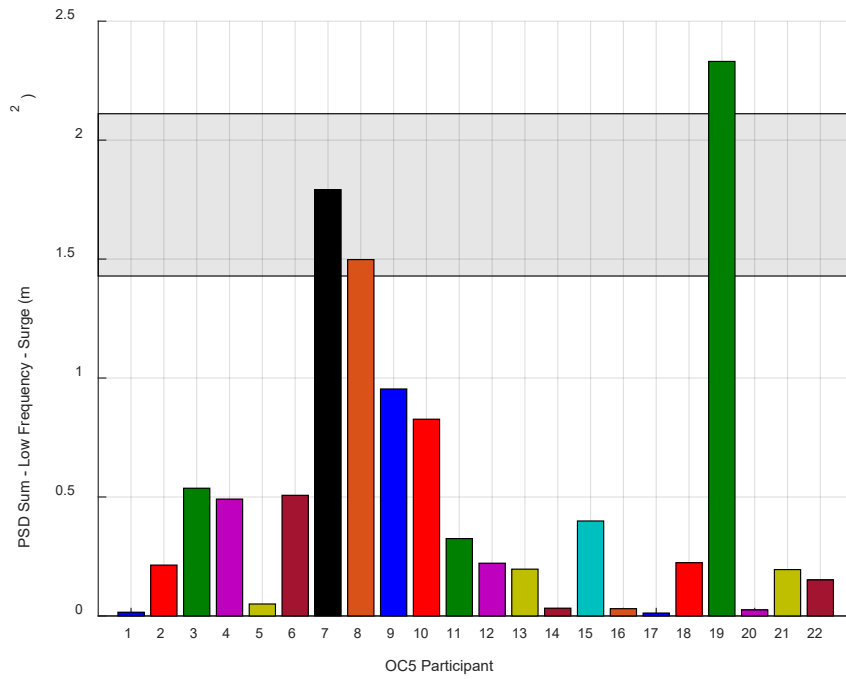


538

539 *Figure 12: Variability of propagated uncertainty for the white noise, low-frequency pitch PSD sum metric, based on a variety of*  
 540 *modelling approaches; positive metric variations are in bold and negative are shown in a muted color*

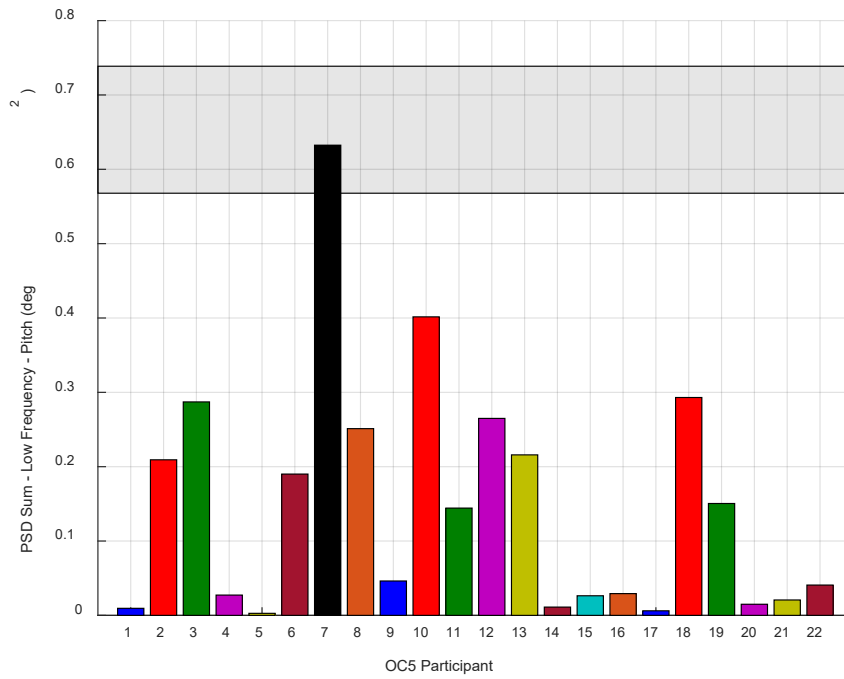
#### 541 6.4 Application to OC5 results

542 In order to understand the magnitude of the experimental uncertainty with respect to numerical  
 543 simulations, the original OC5 study results (Robertson et al. 2017) are re-visited here. The experimental  
 544 tests which were studied in the OC5 project correspond to a different physical model, in a different basin,  
 545 but under similar wave conditions (LC3.3 from Robertson et al. 2017). As shown in Figure 13 and Figure  
 546 14, the PSD sums were computed for both the experimental and numerical results in the OC5 study, and  
 547 the relative uncertainty from the present tests was applied to the original experimental results. For the  
 548 low-frequency surge metric, only one of the numerical results (out of 21 participant results) was within  
 549 the error bounds on the experimental result – even after several iterations and tuning. None of the  
 550 simulation tools predicted the low-frequency pitch response within the experimental uncertainty. It  
 551 should be noted that the tuned PQ approach used for the uncertainty propagation in this paper, which  
 552 shows promise in estimating these low-frequency metrics, is not represented in the OC5 study. This  
 553 modeling approach, as well as others, were developed as a direct consequence of the issues identified in  
 554 OC5.



555

556 *Figure 13: Low-frequency surge PSD sum metric for the original OC5 results (Robertson et al. 2017), with experimental uncertainty*  
 557 *indicated based on the present work. OC5 participant 7 (black) refers to the experimental results.*



558

559 *Figure 14: Low-frequency pitch PSD sum metric for the original OC5 results (Robertson et al. 2017), with experimental uncertainty*  
 560 *indicated based on the present work. OC5 participant 7 (black) refers to the experimental results.*

## 561 7 Conclusions

562 The total experimental uncertainty in a set of hydrodynamics model tests with a rigid semisubmersible  
563 wind turbine has been estimated through propagation of the systematic uncertainties using several  
564 numerical simulation tools. Considering response metrics which give an indication of the wave-frequency  
565 and low-frequency responses of the system, the wave frequency responses are found to have relatively  
566 small uncertainty, while the uncertainty in the low-frequency responses is somewhat higher (20-40% in  
567 the integral of power spectral density over a defined low-frequency range). The random uncertainty,  
568 which was found through repeated measurements, is negligible compared to the estimated systematic  
569 uncertainty.

570 The main contributions to the propagated systematic uncertainty in low-frequency responses were  
571 primarily model characteristics that affected the stiffness: mooring system stiffness for the surge  
572 response, and platform draft, and vertical center of gravity for the pitch response. In addition, uncertainty  
573 in the wave amplitude also had an impact. The simulation tools applied in the study showed good  
574 agreement regarding which parameters were most important, although the magnitude of the propagated  
575 uncertainty differed significantly among participants.

576 A major limitation in the present work is the use of simulation tools for uncertainty propagation: the  
577 inconsistent estimation of the baseline value of the low-frequency PSD sums suggests that the modelling  
578 tools may not be sufficiently accurate to be used for uncertainty propagation. At present, however, these  
579 tools represent the state-of-the-art, and the results of the present study suggest that the differences  
580 between experiments and simulations are larger than the uncertainty in the experimental results.

581 The results from this study give a measurement of uncertainty that can be used in future validation efforts:  
582 the data from the present tests will be studied further using both engineering and high-fidelity models  
583 through the OC6 extension of the Offshore Code Comparison Collaboration through the International  
584 Energy Agency. Additional tests, where wave and radiation loads were measured directly on the fixed  
585 structure, will also be incorporated in the OC6 project in order to better understand the reasons for  
586 discrepancies between simulations and experiments.

## 587 Acknowledgments

588 The authors would like to acknowledge the support of the MARINET2 project (European Union's Horizon  
589 2020 grant agreement 731084), which supplied the tank test time and some travel support to accomplish  
590 the experimental testing campaign. The support of MARIN in the preparation, execution of the model-  
591 tests, and the evaluation of the level of different sources of uncertainties was essential for this study.  
592 MARIN's contribution was partly funded by the Dutch Ministry of Economic Affairs through TKI-ARD  
593 funding programs.

594 This work was partially supported by the U.S. Department of Energy under Contract No. DE-AC36-  
595 08GO28308 with the National Renewable Energy Laboratory. Funding for the work was provided by the  
596 DOE Office of Energy Efficiency and Renewable Energy, Wind Energy Technologies Office.

597 The U.S. Government retains and the publisher, by accepting the article for publication, acknowledges  
598 that the U.S. Government retains a nonexclusive, paid-up, irrevocable, worldwide license to publish or  
599 reproduce the published form of this work, or allow others to do so, for U.S. Government purposes.

## 600 References

- 601 1. ASME (2013). "Test Uncertainty, Performance Test Codes," ASME PTC 19.1-2013.
- 602 2. Berthelsen, P. A.; Bachynski, E. E.; Karimirad, M. and Thys, M. (2016) Real-time Hybrid Model testing  
603 of a Braceless Semisubmersible Wind Turbine. Part III: Calibration of a Numerical Model. in  
604 Proceedings of the ASME 2016 35<sup>th</sup> International Conference on Ocean, Offshore and Arctic  
605 Engineering OMAE2016, Busan, Korea, June.
- 606 3. Buchner et al. (2001). "Numerical Multiple-Body Simulations of Side-by-Side Mooring to an FPSO",  
607 Proc. of IOPEC 2001.
- 608 4. Cermelli CA, Roddier DG. Experimental and Numerical Investigation of the Stabilizing Effects of a  
609 Water-Entrapment Plate on a Deepwater Minimal Floating Platform. ASME. International Conference  
610 on Offshore Mechanics and Arctic Engineering, *24th International Conference on Offshore Mechanics  
611 and Arctic Engineering: Volume 2* (:):517-525. doi:10.1115/OMAE2005-67077.
- 612 5. Clifton, A.; Daniels, M. Lehning, M. (2014). "Effect of winds in a mountain pass on turbine  
613 performance". *Wind Energy* 17 (10) (2014) 1543e1562. Dieck, R. H. (2007). "Measurement  
614 Uncertainty: Methods and Applications (Fourth Edition)," The Instrumentation, Systems, and  
615 Automation Society.
- 616 6. Figliola, R. and Beasley, D. (2011) "Theory and Design for Mechanical Measurements (Fifth Edition),"  
617 John Wiley and Sons, Inc.
- 618 7. Goupee, A. J., Fowler, M. J., Kimball, R. W., Helder, J. and de Ridder, E.-J. (2014) Additional wind/wave  
619 basin testing of the DeepCwind semisubmersible with a performance-matched wind turbine. in  
620 Proceedings of the ASME 2014 33<sup>rd</sup> International Conference on Ocean, Offshore and Arctic  
621 Engineering OMAE2014, San Francisco, California, USA, June.
- 622 8. Goupee, A. J., Koo, B. J., Lambrakos, K. F. and Kimball, R. W. (2012) Model Tests for Three Floating  
623 Wind Turbine Concepts. in Offshore Technology Conference.
- 624 9. Gueydon, S. (2017) MARINET2 OC6 Model-tests MARIN. *To be published on MARIN's website.*
- 625 10. Gueydon, S., Duarte, T., Jonkman, J. Comparison of Second-Order Loads on a Semisubmersible  
626 Floating Wind Turbine. in Proceedings of the ASME 2014 33<sup>rd</sup> International Conference on Ocean  
627 Offshore Mechanics and Arctic Engineering OMAE2014, San Francisco, United States, June.
- 628 11. Gueydon, S., 2016. "Aerodynamic Damping on a Semisubmersible Floating Foundation for Wind  
629 Turbines," *Energy Procedia* (2016) pp. 367-378, DOI: 10.1016.
- 630 12. ISO (1993). "Guide to the Expression of Uncertainty in Measurement," International Standards  
631 Organization, Geneva, Switzerland.

- 632 13. ITTC (2008). "Guide to the Expression of Uncertainty in Experimental Hydrodynamics," Recommended  
633 Procedures and Guidelines, 7.5-01-01.
- 634 14. Jonkman, J. (2010) Definition of the Floating System for Phase IV of OC3.
- 635 15. Jonkman, J., Butterfield, S., Musial, W. and Scott, G. (2009) Definition of a 5-MW Reference Wind  
636 Turbine for Offshore System Development National Renewable Energy Laboratory.
- 637 16. Kim, Y. and Hermansky, G. (2014). "Uncertainties in seakeeping analysis and related loads and  
638 response procedures," *Ocean Engineering*, 86, 68-81.
- 639 17. Masciola, M, Jonkman, J, and Robertson, A (2013). "Implementation of a Multisegmented, Quasi-  
640 Static Cable Model," Proc Twenty-Third International Offshore and Polar Engineering, Anchorage, AK.
- 641 18. Manteufel, R. (2012). "Sequential Perturbation Uncertainty Propagation in Thermal-Fluid  
642 Applications." Proceedings of the ASME 2012 International Mechanical Engineering Congress &  
643 Exposition, Nov. 9-15, 2012, Houston, TX.
- 644 19. Murcia, J.P.; Rethor, P. Dimitrov, N.; Natarajan, A.; Sørensen, J.; Graf, P.; Kim, T. (2016). "Uncertainty  
645 propagation through an aeroelastic wind turbine model using polynomial surrogates." *Renewable  
646 Energy* 2017, <https://doi.org/10.1016/j.renene.2017.07.070>.
- 647 20. Philippe M, Courbois A, Babarit A, Bonnefoy F, Rousset J, Ferrant P. Comparison of Simulation and  
648 Tank Test Results of a Semisubmersible Floating Wind Turbine Under Wind and Wave Loads. ASME.  
649 International Conference on Offshore Mechanics and Arctic Engineering, *Volume 8: Ocean Renewable  
650 Energy*:V008T09A081. doi:10.1115/OMAE2013-11271.
- 651 21. Robertson, A. N., Wendt, F., Jonkman, J. M., Popko, W., Dagher, H., Gueydon, S., Qvist, J., Vittori, F.,  
652 Azcona, J., Uzunoglu, E., Soares, C. G., Harries, R., Yde, A., Galinos, C., Hermans, K., Vaal, J. B. d.,  
653 Bozonnet, P., Bouy, L., Bayati, I., Bergua, R., Galvan, J., Mendikoa, I., Sanchez, C. B., Shin, H., Oh, S.,  
654 Molins, C. and Debruyne, Y. (2017). "OC5 Project Phase II: Validation of Global Loads of the DeepCwind  
655 Floating Semisubmersible Wind Turbine". *Energy Procedia*, Vol 137, pp. 38-57.
- 656 22. Robertson, A. N., Bachynski, E.E., Gueydon, S. Wendt, F., Schünemann, P., and Jonkman, J. (2018).  
657 "Assessment of experimental uncertainty for a floating wind semisubmersible under hydrodynamic  
658 loading." *Proceedings of the ASME 2018 37<sup>th</sup> International Conference on Ocean Offshore Mechanics  
659 and Arctic Engineering*, Madrid, Spain.
- 660 23. WAMIT, Inc. (2011). *WAMIT User Manual Version 6.1, 6.1PC, 6.1S, 6.1S-PC*. Chestnut Hill, MA.
- 661
- 662
- 663